Excellent driven rapid photocatalytic activity with high reusable magnetic nanocomposite in tetracycline degradation under simulated sunlight

Negin Nasseh[a,b], Narjes Sadat Mazari Moghaddam[c,*], Behnam Barikbin[d,*], Rasoul Khosravi[e]

[a]_Cellular and Molecular Research Center, Birjand University of Medical Sciences, Birjand, Iran, email: Negin.Nasseh2020@gmail.com_
[b]_Department of Health Promotion and Education, School of Health, Birjand University of Medical Sciences, Birjand, Iran_
[c]_Environmental Health Engineering, Birjand University of Medical Sciences, Birjand, Iran, Tel.: +9856-32381202;_
_email: narjes_moghaddam1995@yahoo.com_
[d]_Department of Environmental Health Engineering, School of Health, Social Determinants of Health Research Center,_
_Mashhad University of Medical Sciences, Mashhad, Iran, Tel.: +9856-32381202; email: b_barikbin@yahoo.com_
[e]_Department of Environmental Health Engineering, School of Health, Birjand University of Medical Sciences, Birjand, Iran,_
email: Khosravi.r89@gmail.com

ABSTRACT

The present experimental study aimed to determine the efficiency of CuS-coated magnetic activated carbon nanocomposite for the photocatalytic removal of tetracycline (TC) under simulated sunlight. The effects of pH 3, 5, 7, 9, contaminant concentration 5–10–20–50–100 mg/L, nanocatalyst dose 0.025, 0.25, 0.5, 1, 1.5, 2, and 2.5 g/L, and exposure time 1–200 min on the TC removal by the synthesized nanocatalyst were investigated. The maximum removal efficiency was achieved at pH = 9. The TC removal efficiency increased with increasing exposure time and decreasing TC concentration from 100% to 52.1%. The TC removal ratio initially (increased with increasing the nanocatalyst dose from 0.025 to 1.5 g/L (from 37.52% to 89.13%) but started to decrease (54.43%) once the dose was raised above a certain level. The kinetics of the process was found to closely follow the pseudo-first-order kinetic model with $R^2 > 0.9$. After determining the optimal conditions for TC removal with the synthesized nanocatalyst under simulated sunlight, the chemical oxygen demand (COD) and total organic carbon (TOC) removal rates under the same conditions were also experimentally investigated. This investigation showed the COD and TOC removal rates to be 78.13% and 65.81%, respectively. The test results also showed the high recoverability and reusability of the synthesized nanocomposite, with only a 6.08% drop in removal efficiency after six cycles. Also, the effects of some scavenging agents were studied and the results showed the most important role of IPA as a hydroxyl radical scavenger in decreasing the photocatalytic activity of nanocomposite. This confirms that hydroxyl radicals play the most important role in the degradation of tetracycline molecules with respect to e^-/h^+ pairs or $^\bullet O_2^-$. Overall, the results demonstrated the excellent tetracycline removal capability of the synthesized nanocomposite under simulated sunlight.

Keywords: Magnetic nanocomposite; Photocatalytic process; Degradation; Tetracycline; Simulated sunlight

* Corresponding authors.

1. Introduction

Widely used to treat infectious diseases across the world, antibiotics are among the pharmaceutical substances that can be classified as emerging contaminants. Tetracycline (TC) is a broad-spectrum antibiotic that is obtained naturally from the fermentation of certain fungi or through semi-synthetic processes [1]. It is one of the main groups of antibiotics that are commonly used for treating both humans and animals. This antibiotic is extensively used in agriculture as a feed additive [2]. The adsorption of TC by humans and animals could be very low and variable. Unabsorbed TC exerted in the form of non-metabolized compounds, finds its way into domestic and agricultural wastewater, ultimately polluting the environment [3].

Several methods and materials have been proposed for removing TC from water, which include UV light [4], iron nanoparticles [5], adsorption [6], coagulation, Fenton-like catalysts, and other advanced oxidation methods [7,8], photocatalysis [9], nanofiltration [10], carbon nanotubes [11], etc. Each of these processes and materials has certain disadvantages that make them difficult to use. For example, in the adsorption process, the contaminant gets attached to the adsorbent without undergoing any structural change, which means it is only transformed from the soluble phase to the solid phase and remediated without any degradation. Physical processes such as coagulation and centrifugation tend to produce secondary pollutants, which could be problematic [12]. Biological processes are not very effective in removing antibiotics, mostly because of the presence of a stable naphthol ring (as the main structure) in these substances, their toxicity to microorganisms, and their low biodegradability [13].

While other methods such as chlorination, ozonation, advanced oxidation, and nanofiltration can serve as more practical solutions to this problem, they tend to be too expensive and inefficient in the presence of antibiotics [14]. Among the aforementioned methods, photocatalysis could be a top option for TC removal [15]. The use of photocatalysis as a treatment process has attracted increasing attention in recent years thanks to its particularly limited environmental implications [16,17]. The photocatalytic process is a branch of the advanced oxidation process (AOPs). AOPs are based on the production of free and active radicals, especially hydroxyl (OH$^{\bullet}$). These processes are highly effective in removing organic compounds and antibiotics thanks to their high oxidation potential and non-selectivity [18]. Photocatalysts use light to accelerate a reaction that leads to the removal of pollutants and generally require ultraviolet light to operate, this requirement has limited the practical application of most photocatalysts, as 46% of the total light energy. The sun on Earth is in the visible light range and only 4% of it is in the ultraviolet range. Also, considering the problems caused by the cost of supplying ultraviolet light sources in the industry and the high consumption of electricity by these light sources, the introduction of visible light-sensitive photocatalysts can make the path for the industrialization of the use of the photocatalytic oxidation process with the mentioned photocatalysts smoother in the industry. On the other hand, replacing visible light with ultraviolet light can eliminate the harmful effects of UV light [19–21].

Semiconductor photocatalytic processes have many advantages over alternative methods, including excellent degradation efficiency, mineral efficiency, solar energy utilization, low toxicity, low cost, and lack of secondary pollution [22]. Furthermore, this technology offers many economic and social benefits. Researchers have tested many semiconductors, including tungsten trioxide (WO$_3$) [23], cadmium sulfide (CdS) [24], zinc oxide (ZnO) [25], and titanium oxide (TiO$_2$) [26] as catalysts for the photocatalytic degradation of antibiotics. However, WO$_3$ can never be a good catalyst because of low availability, cadmium itself is a toxic heavy metal, and CdS is prone to easy deactivation and photo corrosion [27]. ZnO and TiO$_2$ both have a wide bandwidth, which means they can be activated under the UV region and may not be very efficient under visible light [28]. Copper sulfide (CuS), with a band gap of 2 eV, is a semiconductor compound that can offer excellent physical, chemical, electrical, and magnetic properties for photocatalysis [1]. Nowadays, the removal of pollutants from aquatic environments is carried out using different processes with the help of materials (e.g., activated carbon) and semiconductors (e.g., copper sulfide), some of which can be cited as follows. In separate studies, Ahmad et al. [29] were able to remove volatile organic substances by using carbon materials during the photocatalytic process. In addition, Zhao et al. [30] in a study succeeded in removing tetracycline antibiotics using activated carbon obtained from a mixture of *Phragmites australis* and irrigation sludge.

Although these compounds can increase the efficiency of the photocatalytic process, there are still some unresolved problems regarding their recovery and reusability. One approach to solving this problem is to use catalyst systems based on magnetic nanoparticles. The support considered in this study for this purpose is magnetic activated carbon. While the porous structure, high adsorption capacity, and low price of activated carbon make it a suitable option for removing contaminants from aquatic environments, the large-scale use of this material is hampered by problems related to filtration, dispersion and turbidity, and high regeneration costs [31,32]. The magnetization of activated carbon can facilitate more effective use of this material and help produce an effluent with very low turbidity [33]. However, for magnetic separation of adsorbents, they must be synthesized or combined with nanoparticles, mainly in the form of Fe$_3$O$_4$ magnetic nanoparticles (Fe$_3$O$_4$ MNPs) so that they can be removed from the aqueous medium by a magnet while still attached to the target compound or contaminant. The presence of magnetic iron oxide (Fe$_3$O$_4$) also leads to higher chemical stability, reduced toxicity, and excellent adsorbent recoverability [34].

Activated carbon can be produced from various raw materials, including cellulosic substances such as wood, coconut husk, fruit kernels, and other agricultural wastes, carbon substances such as coal, petroleum coke, and bitumen, and polymeric substances such as waste tires and plastics. Researchers have shown a particular interest in using plants and agricultural by-products in the production of activated carbon to take advantage of their abundance and affordability [35]. In this regard, we can refer to articles such as Sutar et al. [36] and also Assalin et al. [37]. Almond is one of the native plants of South Khorasan, Iran, which

is traditionally cultivated in various parts of this region and plays a notable role in regional commerce and economy. After harvesting the fruit from the tree and removing its green hull, farmers of the region treat this hull as waste, leaving it in the environment; a wasteful practice, potentially polluting, and also creates a visually unpleasant scene.

Considering the potential environmental impacts of antibiotic residues, the proven effectiveness of magnetic nanocomposites in water treatment applications, and the high efficiency of oxidation processes in the removal of organic contaminants, this study evaluated the effectiveness of magnetic activated carbon taken from the almond green hull and coated with CuS (MAC/CuS) in the photocatalytic removal of TC under simulated sunlight.

2. Materials and methods

2.1. Materials

MAC/CuS was synthesized by the use of divalent iron chloride [$FeCl_2 \cdot 4H_2O$] 98%, trivalent iron chloride [$FeCl_3 \cdot 6H_2O$] 98%, sodium hydroxide [NaOH] 80%, concentrated phosphoric acid 85%, hydrochloric acid 37%, copper sulfate [$CuSO_4$] 98%, ethylene glycol [$C_2H_6O_2$] 99%, sodium thiosulfate [$Na_2S_2O_3$] 100% and 99% pure ethanol, all of which were purchased from Merck (Germany). Also, contaminant solutions of different concentrations were prepared by dissolving tetracycline hydrochloride [$C_{22}H_{24}O_8N_2 \cdot HCl$] (Sigma-Aldrich, America) in deionized water.

2.2. Synthesis of magnetic activated carbon

Almond green hull (AGH) was collected and powdered and the resulting powder was passed through a sieve with #60 mesh and again through a sieve with #200 mesh. The powder remaining on the #200 sieve (particles of size 75–250 μ) was collected for use in the production of magnetic activated carbon (MAC). To magnetize the samples, in the first step, 6 g of the sieved powder was mixed with 100 mL of sodium hydroxide and mixed in a shaker at 300 rpm for 30 min. In the second step, 200 mL of distilled water was poured into a two-neck flask and heated to 60°C–70°C on a mixer for 30 min while injecting nitrogen gas was through the second neck. In the third step, 1 g of iron(II) salt and 2 g of iron(III) salt were added to the distilled water on the mixer. In the fourth step, the mixture prepared in the first step was added to the one on the mixer and they were mixed at 60°C and 400 rpm for 1 h. At this point, the nitrogen gas injection was stopped. Finally, the resulting material, which had an alkaline pH, was washed with distilled water until its pH dropped into the neutral range and then dried in an oven at 80°C.

The dried magnetic powder obtained from the previous stage was thoroughly impregnated with 10% phosphoric acid and placed in an isolated environment for 48 h and then dried in a vacuum oven at 75°C for 3 h. It was then transferred into a capped cylindrical steel reactor to prevent oxygen penetration. The steel reactor was placed in a furnace with a programmable HL40P controller, where the temperature was raised to 550°C at a rate of 300°C/h and left there at this temperature for 2 h. Once the furnace cooled

down, the resulting carbon powder was immersed in 3 N HCl and dispersed for 1 h in an Elmasonic E 30H Ultrasonic Unit at a frequency of 37 KHz used as the activating agent.

In this process, 0.15 g of MAC prepared in the previous stage was dispersed in 20 mL of ethylene glycol (EG) for 30 min in an ultrasonic unit and then poured into a 500 cc volumetric flask and placed in an oil bath at 120°C. Next, 0.8 g of $CuSO_4$ was added to this suspension and was completely dissolved in the flask's contents. Then, 1.9 g of $Na_2S_2O_3$, which was mixed in advance, with 20 mL of EG and poured into the suspension containing MAC and copper sulfate, and they were refluxed at 140°C for 90 min. After this period and once the volumetric flask cooled down, the product was separated using an N_{42} magnet and washed once with ethanol and several times with deionized water, and finally dried in an oven at 80°C for 5 h [38].

2.3. Characterization of the synthesized nanocomposites

Field-emission scanning electron microscopy (FE-SEM) was performed with a ZEISS Sigma VP FE-SEM unit (ZEISS, Germany) to study the morphology, shape, average diameter, and size of the synthesized MAC/CuS nanocomposites in micro and nano scales. Specific surface area, porosity, pore volume, and pore size were measured by a BELSORP MINI Automatic Brunauer–Emmett–Teller (BET) Surface Analyzer (MicrotracBEL Corp. Co., Japan). X-ray diffraction (XRD) spectroscopy was performed with an X'Pert Pro XRD unit (PANalytical Co., The Netherlands) to investigate the composition and crystal structure of the synthesized MAC/CuS nanocomposites. The magnetization of the synthesized nanoparticles was measured with a vibrating-sample magnetometer (VSM) model LBKFB (Meghnatis Daghigh Kavir Co., Iran). Also, electrochemical impedance spectroscopy (EIS) analysis was performed to determine electronic properties such as charge transfer resistance, recombination resistance, the diffusion coefficient of charge carriers, diffusion length, chemical capacity by Potentiostat-Galvanostat device, model PGE-18 (Sharif Solar Co., Iran). Energy-dispersive X-ray spectroscopy (EDX) was performed with a ZEISS Sigma 500 VP EDX unit (ZEISS, Germany) to determine the type and proportion of the constituting elements of the synthesized catalyst. Also, diffuse reflectance spectroscopy (DRS) was performed using an AvaSpec-2048TEC unit with AvaLight-DH-S (Scinco Co., South Korea) set up to examine the interaction of light and synthesized material.

2.4. Photocatalytic TC removal tests

For photocatalytic TC removal tests, first, a stock solution (1,000 mg/L) of TC hydrochloride salt in deionized water was prepared. This solution was synthesized weekly and stored in a refrigerator at 4°C. The variables of interest in this study were pH (3, 5, 7, 9), contaminant concentration (5–100 mg/L), nanocatalyst dose (0.025–2.5 g/L), and exposure time (5–200 min). The pH of the solution was adjusted with 0.1 N HCL and NaOH with the help of a pH meter (Knick 766 Calimatic, Germany). All tests were performed in a batch reactor at room temperature (24°C ± 2°C) for 400 mL samples at a mixing speed of 300 rpm under a

500-W Xenon light with a 420 nm filter acting as a sunlight simulator.

It should be noted that before performing the tests under simulated sunlight, the adsorption and desorption reactions of TC were investigated by stirring the mixture of contaminant and magnetic nanocomposites at 300 rpm for 30 min on the magnetic stirrer in a dark environment. After this process, concentration was measured again (54.33%) and the new value was considered as the initial concentration of the photocatalytic process.

Samples were taken at regular intervals. After the separation of the nanocomposite by a magnet, the residual TC concentration was measured by a spectrophotometer (UV/visible T80þ) at 358 nm [39].

The efficiency of the TC removal process was calculated using Eq. (1).

$$Removal\% = \left(1 - \frac{C_t}{C_0}\right) \times 100 \tag{1}$$

where C_0 is the initial concentration of TC (mg/L), C_t is the concentration of TC at time t (mg/L), and $R\%$ denotes the percentage of contaminant removal.

2.5. Determination of adsorbent surface charge (pH_{zpc})

For this measurement, a 0.01 M NaCl solution (0.588 g in 1,000 cc of distilled water) was prepared (to be used as an electrolyte) and 600 mL of it was poured into six Erlenmeyer flasks (100 mL each). The pH of the solutions was adjusted to 2–12 with 0.1 M HCL and NaOH. The solution in each flask was mixed with 0.2 g of the synthesized MAC/CuS nanocomposite and placed on a shaker at 300 rpm for 24 h. After this time, the final pH of the solutions was measured, pH_{final} was plotted against the $pH_{initial}$, and the isoelectric point was determined from the intersection of the curves [40].

2.6. Determination of reaction kinetics

When studying catalytic wastewater treatment processes, especially those involving pharmaceutical contaminations, it is important to investigate reaction kinetics. The rate of heterogeneous catalytic reactions can be generally described by several models, however, the widely used model in the studies of the degradation of a variety of pharmaceutical compounds is the pseudo-first-order.

Eq. (2) shows the simplest form of this model.

$$\frac{C_t}{C_0} = e^{-k_0 \times t} \tag{2}$$

where the k_0 refers to the pseudo-first-order reaction rate constant (min^{-1}).

2.7. Nanocomposite recovery and reuse tests

Stability and reusability are important properties for solid catalysts to be used in treatment applications. To investigate the reusability of the synthesized nanocomposite, six cycles of TC removal were performed under Xenon light using the optimal conditions obtained from the photocatalytic tests. In each cycle, the nanocatalyst was separated from the solution by an N_{42} magnet and washed several times with deionized water and dried in a vacuum oven at 80°C and then used as the catalyst for the next cycle. At the end of each cycle, the residual concentration of the contaminant was measured [41].

2.8. Chemical oxygen demand and total organic carbon tests under optimal conditions

Chemical oxygen demand (COD) and total organic carbon (TOC) tests were performed using methods 5310B and 5220D as instructed in the handbook of Standard Methods for the Examination of Water and Wastewater [42] using an SGE ANA TOC Unit (Australia) and a Lovibond VARIO COD Checkit Direct Unit (Germany).

3. Results and discussion

3.1. Characteristics of the synthesized nanocomposite

3.1.1. XRD analysis

Fig. 1 shows the XRD pattern of the MAC/CuS nanocomposite along with the introduction of the peaks related to the presence of iron (ICSD 159976) and copper sulfide (ICSD 158743) separately.

Using the Scherrer equation based on the full-width at half maximum (FWHM), the size of the synthesized nanocomposite was calculated to be 29 nm. However, in the FE-SEM analysis, it was found that the obtained nanoparticles tend to accumulate because of their magnetic properties and the particle size was calculated to be 64 nm. This difference may be because while XRD analysis generally measures the crystal size, FE-SEM shows the size of the particle, which can consist of several crystals.

$$D = \frac{0.98\lambda}{\beta \cos\theta} \tag{3}$$

where D is the particle diameter, β is the peak width at half height, θ is the diffraction angle at the peak location, λ is the wavelength of the X-ray of the device ($\lambda = 0.1540$ nm).

3.1.2. DRS analysis

DRS analysis was performed to study the optical properties of the nanocomposite. While research has shown that copper sulfide alone has a band gap of 2 eV, this analysis showed that the presence of other materials in the synthesized MAC/CuS slightly changed the band gap of copper sulfide (band gap = 2.3 eV). Therefore, as stated in the authors' previous study [38], the catalyst showed a stronger absorption in the range of 400–700 nm, which is indicative of the suitability of the synthesized nanocomposite for photocatalytic processes in the range of visible light and sunlight.

3.1.3. FE-SEM analysis

Fig. 2a displays a FE-SEM micrograph of AGH at 1000KX magnification. In this figure, it can be seen that the
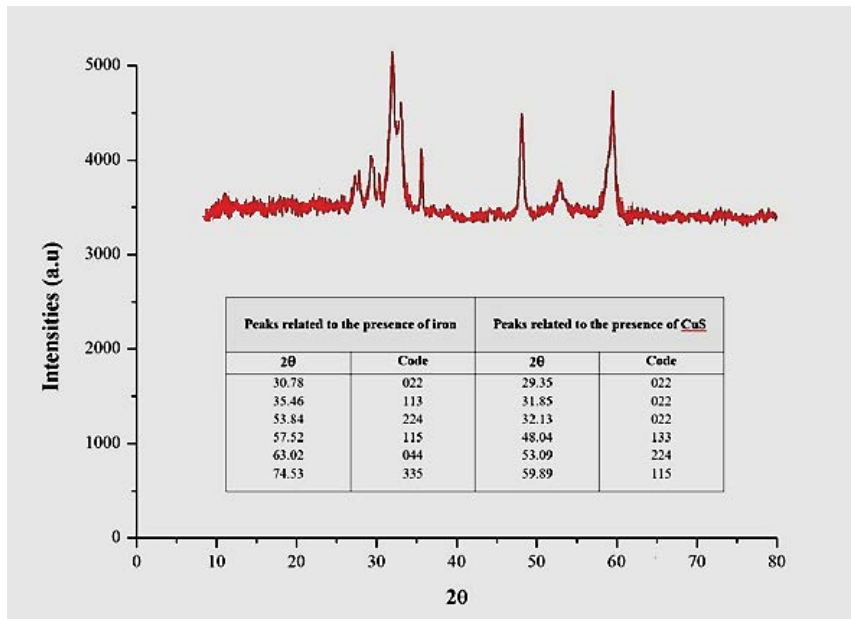
Fig. 1. X-ray diffraction pattern of MAC/CuS.
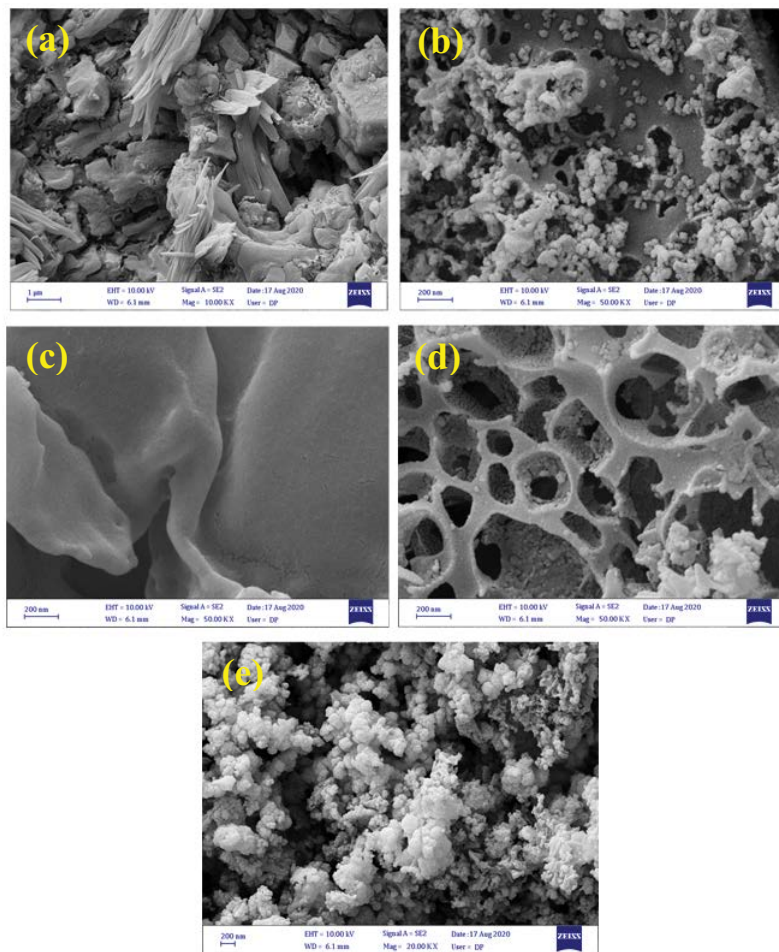
Fig. 2. Images of (a) AGH, (b) magnetic AGH, (c) carbon from magnetic AGH, (d) MAC and (e) MAC/CuS FE-SEM.

adsorbent surface has some pores and cavities. In Fig. 2b, which displays the surface of magnetic AGH, iron particles perfectly and almost uniformly cover the hull surface. In Fig. 2c, which shows the surface of carbon obtained from magnetic AGH, there are very few cavities on the surface of this precursor. Fig. 2d displays an image at 5000KX magnification of the magnetic carbon (MC) obtained from AGH after its activation. As this image shows, with the activation of the carbon obtained from the burning of magnetic AGH, extensive regular cavities appeared on its surface. After adding hydrochloric acid and performing an ultrasound, major changes occurred in the fractures and subsurface layers. As mentioned, the innovation of this study compared to other studies that have used activated carbon is the use of ultrasound in the process. The use of ultrasound in aqueous media leads to cavitation, which results in the production of free radicals in the environment. These radicals penetrate the solution, causing organic compounds to undergo oxidation. During the cavitation process, the penetration of solvent vapor into the bubble causes it to burst, which releases energy and allows chemical reactions, including chelating, to take place. As these figures show, AGH itself has a uniform surface with a few pores and cavities, but the surface pores increase as it is processed into activated carbon. Fig. 2d clearly shows the presence of cavities of different sizes with an almost uniform distribution on the surface. Fig. 2e displays an image of the MAC/CuS composite obtained after introducing copper sulfide to the activated carbon from AGH with a 2000KX magnification. As this figure illustrates, copper sulfide desirably covered the activated carbon.

3.1.4. EDX analysis

The results of the EDX analysis of AGH are provided in Fig. 3a, which clearly shows the presence of C and O in this substance. Fig. 3b also shows the presence of iron on the hull in a 1 to 3 ratio. The EDX analysis of the carbon obtained from magnetic AGH in Fig. 3c shows a significant reduction in carbon content after burning. The EDX image of the final composite is presented in the authors' previous paper [38].

3.1.5. VSM analysis

The magnetic properties of the synthesized nanocatalyst were investigated with the help of a VSM. The results of the VSM analysis of magnetic MAC and MAC/CuS are presented separately in Fig. 4. These diagrams demonstrate the good magnetic properties of the synthesized nanoparticles and nanocomposites. The magnetic saturation of MAC and MAC/CuS was calculated to be 17 and 11.1 emu/g, respectively. As the VSM results demonstrate, the greatest magnetic property was observed in the activated carbon obtained from magnetic AGH. carbonation turns many organic compounds of the green hull into bituminous materials, which remain on the surface of the catalyst, reducing its magnetic properties and with the activation process removes these bituminous materials from the catalyst and so leading to a significant strengthening of magnetic effects. With the introduction of copper sulfide to the obtained activated carbon, its magnetic properties slightly decreased. However, it still disperses well in water and can be easily
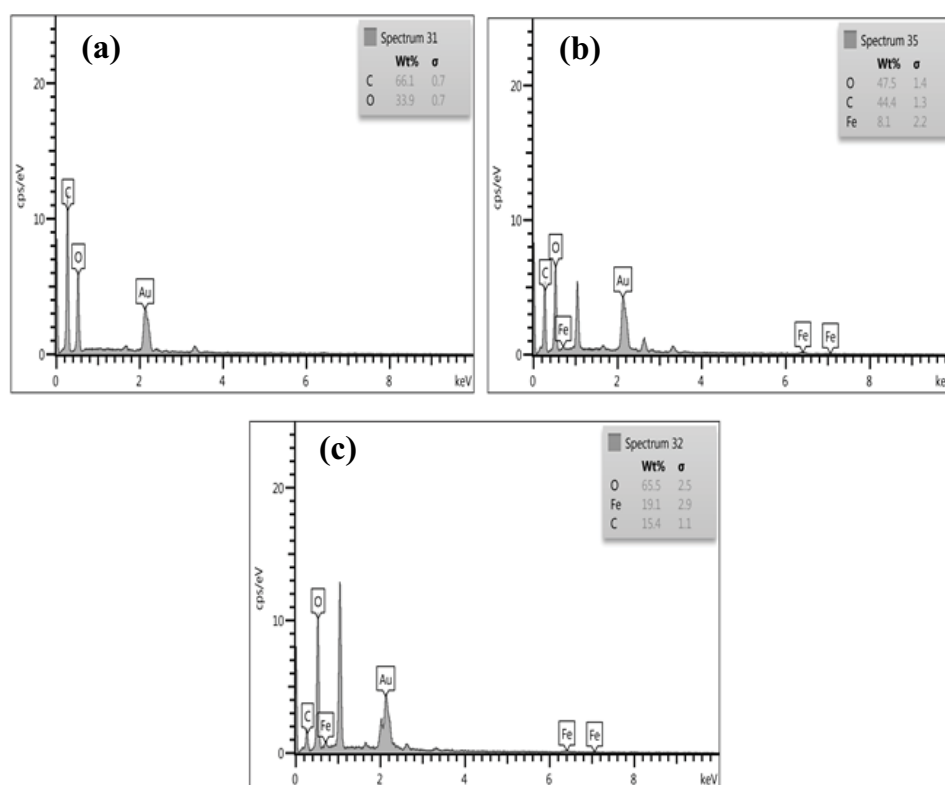
Fig. 3. Energy-dispersive X-ray spectroscopy analysis of (a) AGH, (b) magnetic AGH and (c) carbon from magnetic AGH.
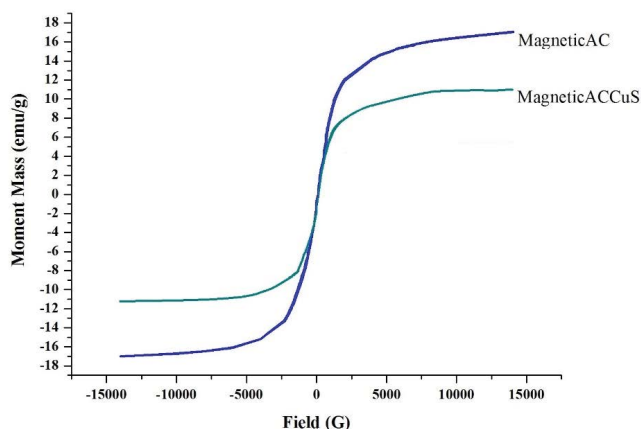
Fig. 4. Vibrating-sample magnetometer analysis of MAC and MAC/CuS.

Fig. 5. Electrochemical impedance spectroscopy Nyquist plots of CuS and MAC/CuS nanocomposite.

and rapidly collected by an external magnetic field and then re-dispersed with a little shaking.

3.1.6. EIS analysis

EIS spectra of CuS and nanocomposite MAC/CuS were measured to further confirm the charge transfer resistance. EIS spectra of pure CuS and nanocomposite MAC/CuS were measured to further confirm the charge transfer resistance. Their EIS Nyquist plots are presented in Fig. 5. The diameter of the semicircle represents the load isolation resistance, and the smaller arc radius means better isolation efficiency of the optical carrier [43]. As it is clear from these graphs, nanocomposite MAC/CuS has the lowest radius compared to CuS, which shows that nanocomposite MAC/CuS has the lowest resistance and the highest charge separation efficiency. A decrease in resistance can be caused by an increase in the level. One of the effects of increasing the level is the increase in the number of load carriers; That is, with the development of the active surface, the amount of light absorption is higher and as a result, the number of charge carriers is increased.

3.1.7. BET analysis

The results of the BET analysis showed that the activation process significantly increased the specific surface area. These results demonstrated the effectiveness of ultrasonic waves in improving the specific surface area of carbon. As the data obtained from this analysis show, the specific surface area of raw AGH powder was only 13.032 m^2/g, which can be attributed to the presence of a few pores on its relatively smooth surface, as was also observed in the related FE-SEM images. After carbonizing the magnetic powder, its specific surface area further decreased to 8.44 m^2/g. This is because of the transformation of organic compounds into bituminous materials on the adsorbent surface in the absence of oxygen, which further reduced its roughness. This is also indicative of the proper carbonation of the material. Once carbon was activated, the specific surface area increased to 186.83 m^2/g. This indicates that the activation process has perfectly removed the said bituminous materials from the
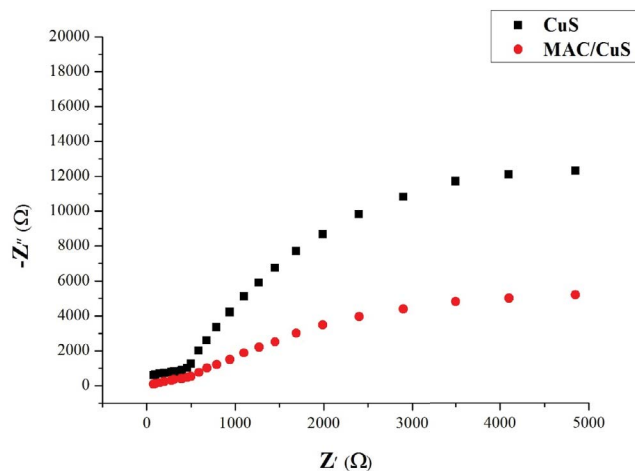
surface, changing it so that the outcome is a remarkable increase in the surface-to-volume ratio. The FE-SEM results also confirm this change. According to the results of the BET analysis, introducing CuS to the magnetized composite significantly decreased its specific surface area (to 14.79 m^2/g); an effect that can be attributed to the deposition of copper sulfide particles on the composite surface and its cavities. The morphological change of the composite after CuS deposition is also clearly visible in the FE-SEM images.

The average pore size of AGH, MC, MAC, and MAC/CuS was measured at 3.75, 20.32, 7.92, and 39 nm, respectively. Carbonizing AGH involves burning its volatile organic matter at 500°C under anaerobic conditions; a process that creates many cavities on its surface. However, as mentioned, some of these incinerated materials become bituminous and cover the cavities, which results in higher average pore size in carbonized AGH. During the activation process, the combination of ultrasound and dilute hydrochloric acid solution detaches these bituminous materials from the adsorbent surface, increasing the cavities and consequently decreasing the average pore size to 7.92 nm. Finally, with the deposition of CuS on MAC, the average pore size increases dramatically. Fig. 6 shows the adsorption and desorption isotherms of the synthesized composite.

3.2. Parameters affecting the photocatalytic degradation of TC

3.2.1. Effect of pH

Many researchers have identified pH as an important determinant of the effectiveness of advanced oxidation processes (AOPs) in antibiotic removal. This is because pH has a great impact on the distribution of electric charge on the photocatalyst surface, contaminant decomposition rate, adsorption capacity, and valence band oxidation potential [44,45]. In this study, the highest photocatalytic TC removal efficiency was achieved in alkaline media (Fig. 7a). As many studies have explained, TC is an amphoteric molecule consisting of three functional groups: tricarbonyl methane group, phenolic diketone group, and dimethyl amino group. The acidity constant (pK_a) of these functional groups in

aqueous media change with pH so that they are protonated in highly acidic environments (pH < 4), uncharged in acidic to neutral environments (4 < pH > 7.5), and anionic in neutral to alkaline environments (7.5 < pH > 10) [4,46,47]. As a result, TC decomposition rate and efficiency change with pH depending on which component of this antibiotic is predominant. The photocatalytic degradation process is least effective when the TC is mostly made of the tricarbonyl methane group and is most effective when TC is mostly made of the dimethyl amino group. TC has a higher electron density in alkaline media than in acidic media, and it is more open to the attack of radical species in the former [48,49]. The effect of pH on photocatalytic TC degradation has been investigated in many studies, and all of these; the highest oxidation capacity has been achieved in the range of neutral to alkaline pH. The present study also reached the same conclusion, as the results showed only 11.71% contaminant removal after 60 min at pH = 3, but this value was 31.29% at pH = 7 and 57.62% at pH = 9. This result is consistent with the findings of Xue et al. [49] and Ma et al. [50].

Determining the isoelectric point (pH_{zpc}) can also prove valuable for predicting the behavior of the synthesized nanocomposite. The iso-electric point (pH_{zpc}) of this nanocomposite was found to be about 7. As mentioned at the beginning of this subsection as well as in many other studies, TC molecules tend to take a positive charge in acidic environments. The results of this study suggested that the synthesized magnetic nanocomposite also had a positively charged surface in acidic pH, and therefore, because of the repulsive force created between TC and MAC/CuS, the nanocomposite showed a lower TC adsorption capability in the acidic environment [51–54].

Also, the synthesized nanocomposite particles showed a greater tendency to accumulate and agglomerate in acidic pH, which result in a lower contaminant removal rate. According to many sources, the most important oxidation agents in neutral and alkaline pH are OH• radicals produced by the reaction between hydroxide ions (OH⁻) and positive holes [55]. But in acidic pH, this role is played exclusively by positive holes [51,56]. Therefore, because of the positive charge of the amine group in the TC molecule of dimethyl amino type and the negative charge of the catalyst surface in alkaline pH, an alkaline environment enhances the attraction of this contaminant to the adsorbent molecules, thereby increasing the efficiency of the photocatalytic process.

Since pH changes could have unintended impacts on the nanocomposite structure, before running the tests, this possibility was investigated by placing the synthesized nanocomposite in different pH (3, 5, 7, and 9) for 60 min, and then conducting a Fourier-transform infrared spectroscopy analysis. The results of this analysis are presented
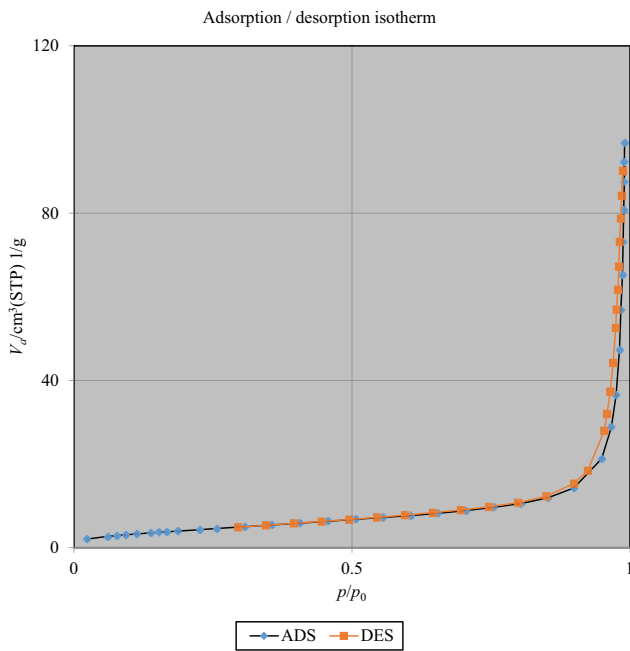
Fig. 6. Adsorption/desorption isotherm of Brunauer–Emmett–Teller analysis.
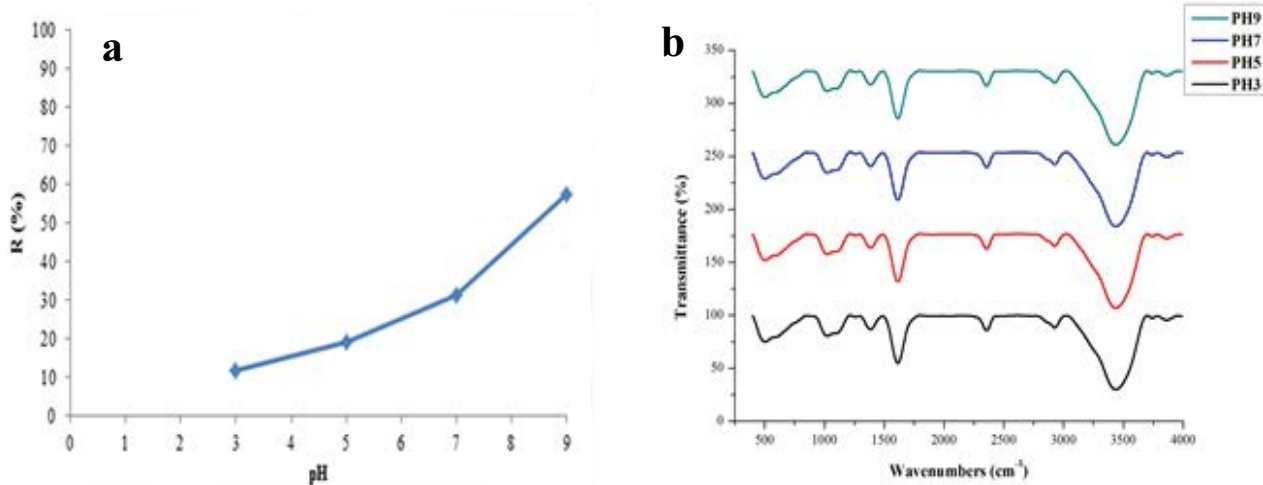
Fig. 7. (a) Effect of pH on tetracycline degradation with the synthesized MAC/CuS composite under Xenon light (tetracycline concentration = 20 mg/L, catalyst dose = 0.25 g/L, ambient temperature) and (b) assessment of the stability of the synthesized MAC/CuS composite at different pHs using Fourier-transform infrared spectroscopy.

in Fig. 7b. This analysis showed that pH did not affect the structure of the nanocomposite.

3.2.2. Effect of magnetic nanocomposite dose

Another important determinant of the efficiency of antibiotic removal through photocatalytic processes is the dose of the synthesized catalyst. To investigate the effect of the dose on the rate of TC removal, a series of TC removal tests were performed with different doses of the synthesized MAC/CuS composite (0.025, 0.25, 0.5, 1, 1.5, 2, and 2.5 g/L). These tests were performed under Xenon light on a TC solution with a concentration of 20 mg/L at the optimum pH (pH = 9). Contrary to our initial expectation, the results showed that as the MAC/CuS dose increased, the TC removal efficiency initially increased but then started to decrease as shown in Fig. 8a. For example, the TC removal rate achieved with the MAC/CuS doses of 0.025, 1.5, and 2.5 g/L after 60 min was 37.52%, 89.13%, and 54.43%, respectively. This could be because as the catalyst dose increases, so does the turbidity of the solution, which can decrease the process efficiency by reducing light transmission. This
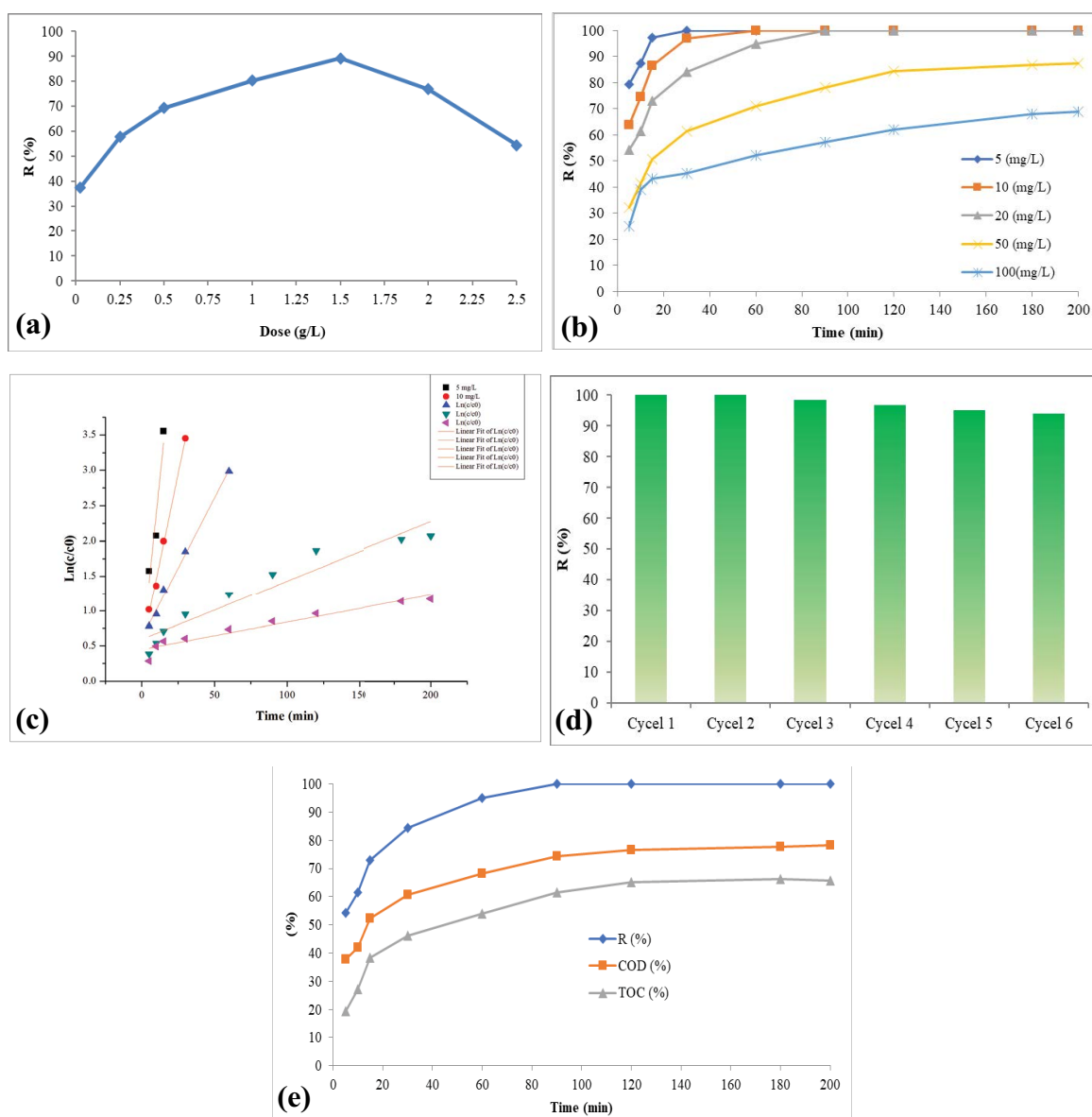
Fig. 8. (a) Effect of the dose of the synthesized MAC/CuS nanocomposite on tetracycline removal under Xenon light (tetracycline concentration = 20 mg/L, pH = 9, ambient temperature), (b) effect of initial tetracycline concentration on tetracycline removal with the synthesized MAC/CuS nanocatalyst (MAC/CuS dose = 1.5 g/L, pH = 9, ambient temperature), (c) kinetics of tetracycline degradation with the synthesized MAC/CuS nanocatalyst, (d) results of six cycles of photocatalytic tetracycline degradation with the synthesized MAC/CuS nanocatalyst under Xenon light (tetracycline concentration = 20 mg/L, MAC/CuS dose = 1.5 g/L, exposure time = 200 min, pH = 9) and (e) chemical oxygen demand and total organic carbon removal efficiency of the synthesized MAC/CuS nanocatalyst under optimal conditions (Tetracycline concentration = 20 mg/L, MAC/CuS dose = 1.5 g/L, pH = 9, ambient temperature).

argument is consistent with the results of Eslami et al. [57] and Xue et al. [49]. The second reason for this trend could be the agglomeration or precipitation of the nanocomposite particles because of the stronger magnetic property at higher doses, which leads to a decrease in the number of active sites available for photon adsorption [58]. Based on these test results, the optimal dose of the synthesized MAC/CuS nanocomposite for TC removal under Xenon light is 1.5 g/L. It should be noted that there is a strong possibility of achieving lower removal rates with this dose in real wastewater because of the lower light penetration and the presence of interfering anions such as bromine, phosphate, chloride, and sulfate. The above results are consistent with the findings of other studies on the photocatalytic degradation of tetracycline [49], amoxicillin, ampicillin, cloxacillin [59], 2-chlorophenol [58], and phenolic compounds [60].

3.2.3. Effect of TC concentration and exposure time

To investigate the effect of initial TC concentration and exposure time on photocatalytic removal efficiency, a series of tests were conducted with different TC concentrations (5, 10, 20, 50, and 100 mg/L) and exposure times. These tests were carried out under Xenon light using the optimal MAC/CuS nanocatalyst dose (1.5 g/L) and optimal pH condition (pH = 9). The results of these tests are illustrated in Fig. 8b. These tests showed that the TC removal efficiency drops sharply as the initial TC concentration increases. For example, the TC removal rates achieved after 60 min with the initial TC concentrations of 20, 50 and 100 mg/L were 94.93% and 71.6%, 52.1%, respectively. Since these results were obtained under constant conditions in terms of MAC/CuS nanocomposite dose, exposure time, pH, and light lux, they indicate that having lower concentrations of TC in the environment results in more reaction between TC and $OH^{\bullet}$ radicals and electron holes, which ultimately leads to better degradation of this contaminant by free radicals. A higher TC concentration also lowers contaminant degradation by allowing less light to reach catalyst particles. This relationship can also be related to the rate of adsorption of contaminants on the catalyst, because as the TC concentration increases, the said rate also increases, and consequently the catalyst's light absorption efficiency decreases. These results are consistent with the finding of a study by Rezaei et al. [61], where photocatalytic TC removal was carried out by magnetic carbon-supported TiO_2 nanoparticles catalyzed peroxydisulfate. It should be noted that visible light radiation alone did not have a significant impact on TC removal (less than 30% after 200 min) [62].

3.3. Photocatalytic TC degradation kinetics

Following the approach of similar studies, the kinetics of TC degradation with the synthesized MAC/CuS nanocomposite under sunlight was investigated by the use of the pseudo-first-order kinetic model [59]. For this purpose, the authors used the test results obtained for TC concentrations of 5, 10, 20, 50, and 100 mg/L with a MAC/CuS dose of 1.5 g/L, pH of 9, and exposure time of 60 min [63]. These results are presented in Table 1 and illustrated in Fig. 8c. This investigation showed that the reaction rate constant (K_{obs}) significantly decreases as TC concentration increases. It was also found that the pseudo-first-order kinetic model is a suitable model for describing the kinetics of this reaction and can predict the test results for all TC concentrations with a coefficient of determination (R^2) close to 1. The observed relationship between K_{obs} and TC concentration could be related to the relatively limited number of active hydroxyl radicals available at higher TC concentrations because of the increased concentration of intermediate products, which results in a reduced degradation rate [64].

3.4. Reusability of the synthesized MAC/CuS nanocatalyst in the photocatalytic TC degradation process

The authors also investigated the reusability of the synthesized MAC/CuS nanocomposite in photocatalytic TC degradation. For this purpose, six cycles of TC removal were performed under Xenon light. Each of these cycles involved using the nanocomposite for TC removal for 200 min, separating it from the solution by a magnetic field, washing it with distilled water and ethanol, drying it in a vacuum oven for 8 h at 80°, and using the product in the next cycle. The results of this process are illustrated in Fig. 8d. In the sixth cycle, the nanocomposite showed about a 6% efficiency reduction compared to the first cycle. This performance reduction can be attributed to the reduced quantity of the catalyst (5% of the catalyst cannot be recovered by magnetic field) as well as structural change in the catalyst due to light reactions [65]. The TC degradation rate at the end of the sixth cycle was about 93.92%. It was observed that the synthesized nanocomposite can be rapidly separated from the solution by applying an external magnetic field; a property that greatly facilities recovery and reuse. Magnetic separation could be preferable over recovery methods that involve filtration or centrifugation, as these methods can become excessively time-consuming or expensive. Magnetic separation also has lower mass loss than other conventional

Table 1
Parameters of the pseudo-first-order kinetic model for tetracycline degradation

Concentration (mg/L)	Equation	k_0 (min^{-1})	R^2	$t_{1/2}$ (min)
5	$Y = 0.1978x + 0.4213$	197.8×10^{-3}	0.9247	3.50
10	$Y = 0.0993x + 0.4689$	99.3×10^{-3}	0.9959	6.99
20	$Y = 0.0398x + 0.6179$	39.8×10^{-3}	0.9951	17.41
50	$Y = 0.0084x + 0.5935$	8.4×10^{-3}	0.9202	82.5
100	$Y = 0.0039x + 0.4477$	3.9×10^{-3}	0.9319	177.69

$t_{1/2} = 0.693/k_0$

separation methods, which can have a significant impact on the recovery cost.

3.5. COD and TOC reduction efficiency under optimal conditions

Fig. 8e shows the COD and TOC removal efficiency of the synthesized nanocomposite under optimal conditions (TC concentration = 20 mg/L, MAC/CuS dose = 1.5 g/L, pH = 9, ambient temperature) for different exposure times. As can be seen, after 200 min under optimal conditions, the process achieved 100% TC removal, 78.13% COD removal, and 65.81% TOC removal. The difference between these figures can be attributed to the incomplete degradation of TC and its partial transformation to organic intermediary products, which result in relatively lower TOC and COD removal rates. In other words, while a major portion of the antibiotic completely breaks down into the expected mineral compounds, that is, H_2O and CO_2, the rest of it turns into organic by-products [57].

3.6. TC removal mechanism

Semiconductors are used in photocatalytic reactors because of having conduction and valence bands separated by a band gap. The photocatalytic process of this study progresses as follows. First, the catalyst particle absorbs a photon with energy equal to or greater than its band gap, which results in the creation of an electron–hole pair following the excitation of the electron from the valence band to the conduction band [Eq. (4)]. At this point, there is an electron pair in the conduction band and a hole in the valence band. Because of the high oxidation potential of the hole, it engages in redox reactions with particles adsorbed on the catalyst surface, such as water, OH^- and oxygen, creating hydroxyl radicals [Eqs. (5) and (6)]. The produced electrons also get trapped by dissolved oxygen, producing superoxide ions (O_2^-) and other active oxygen species such as hydrogen peroxide [Eqs. (7)–(9)]. Hydrogen peroxide produces more free radicals through a series of reactions [Eqs. (10)–(12)] [66,67]. These reactions are available in an article published by Nasseh et al. [38].

Fig. 9 depicts the mechanism of the photocatalytic removal process of tetracycline using the nanocomposite synthesized in this study with the reactions taking place in this process.

3.7. Effect of scavenging agents

To show the relative roles of the main electron/hole (e^-/h^+) pairs active species, $^\bullet OH$ and $^\bullet O_2^-$ in the photodegradation of TC, experiments were performed in the presence of a concentration of 20 mg/L of some scavenger species and at the optimal time of this process, 60 min. The scavengers studied in this research were ethylenediaminetetraacetic acid (EDTA) (hole scavenger), potassium peroxydisulfate (electron scavenger), chloroform ($^\bullet O_2^-$ scavenger) and isopropyl alcohol (IPA) ($^\bullet OH$ scavenger).

The results are summarized in Fig. 10. As can be seen, in the presence of most of the scavenger agents except potassium peroxydisulfate, the decomposition efficiency
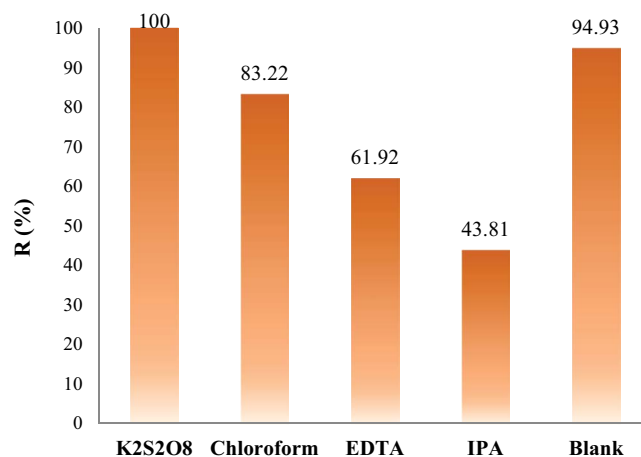
Fig. 10. Effects of different scavenging agents on the photocatalytic activity of MAC/CuS in tetracycline photodegradation (dose of MAC/CuS: 1.5 g/L, pH: 9, C TC: 20 mg/L, contact time: 60 min, C scavenger: 20 mg/L).
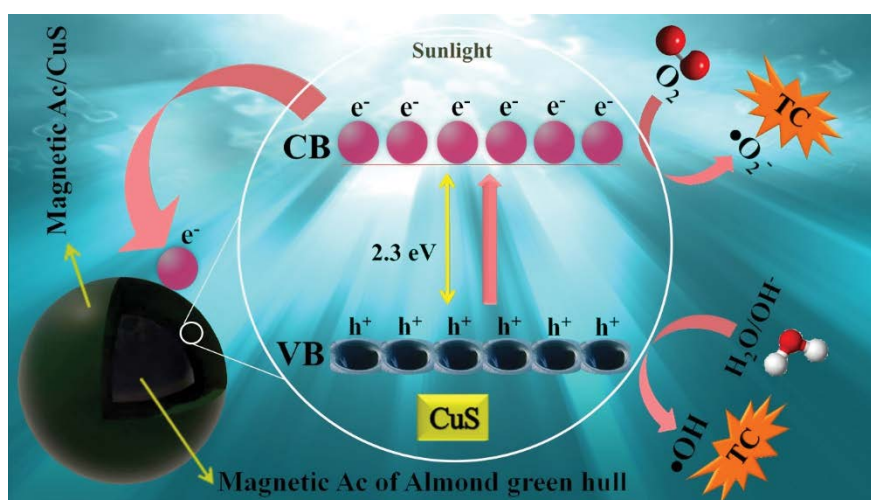
Fig. 9. Photocatalytic removal mechanism of tetracycline.

decreases, and the most decrease in the decomposition efficiency is observed by IPA, which is a $^\bullet$OH scavenger, which confirms the vital role of $^\bullet$OH and then the photogenerated holes in the photodegradation of TC. Finally, the radical $^\bullet O_2^-$ and photogenerated electron, respectively play the next roles in the optical degradation of TC.

3.8. TC degradation pathway during the MAC/CuS/Xenon photocatalytic process

To investigate the fate of TC in the MAC/CuS photocatalytic process in the presence of simulated sunlight, the contaminant was exposed to the optimal conditions determined in the previous steps and then analyzed by an Agilent 5979-C GC-MASS unit. The results showed that this process led to the production of phthalic acid mono-2-ethylhexyl ester, 4,8,12-tetradecatrienal, 5,9,13-trimethyl, heptane, 2,2,6,6-tetramethyl-4-methylene, 3,8-dimethyldecane, decane, 4-ethyl- and 2-methylpentane (Table 2). As shown in Table 2, TC first turns into simpler cyclic compounds and then into linear organic contaminants, eventually converting into carbon dioxide and water. The efficiency of different processes of photocatalyst, adsorption and photolysis were also compared in the removal of TC and the results are shown in Fig. 11.

Table 2
Tetracycline degradation pathway the MAC/CuS/Xenon photocatalytic process

No.	Compound name	Structure	Retention time (min)	Main fragments
1	Phthalic acid mono-2-ethylhexyl ester		13.9	82 (82%), 69 (69%), 55 (55%), 41 (41%)
2	4,8,12-Tetradecatrienal, 5,9,13-trimethyl		16.37	92 (98%), 77 (82%), 65 (69%), 51 (54%), 31 (33%)
3	Heptane, 2,2,6,6-tetramethyl-4-methylene		20.54	91 (66%), 77 (56%), 65 (47%), 51 (37%)
4	3,8-Dimethyldecane		24	127 (99%), 113 (88%), 99 (77%), 85 (66%), 71 (55%), 57 (44%), 43 (33%)
5	Decane, 4-ethyl-		27.3	85 (58%), 71 (57%), 57 (70%), 41 (42%), 39 (11%)
6	2-Methylpentane		31.89	71 (28%), 57 (10%), 86 (7%)

Table 3
Degradation effect of different catalysts on tetracycline

Nanocatalyst	pH	Dose (g/L)	Initial concentration (mg/L)	Time (min)	Lamp type	Removal (%)	References
FeNi$_3$/SiO$_2$/ZnO	9	0.02	20	200	Xenon	100	[68]
AgI	9	0.01	20	180	Xenon	97.91	[69]
MAC/CuS	9	1.5	20	200	Xenon	94.93	This study

Compared to the previously reported studies, this MAC/CuS photocatalyst shows a much higher photocatalytic ability for organic pollutants under visible light than many other photocatalysts (Table 3).

3.9. Comparison of different processes of photocatalyst, absorption, and photolysis in the removal of tetracycline antibiotic
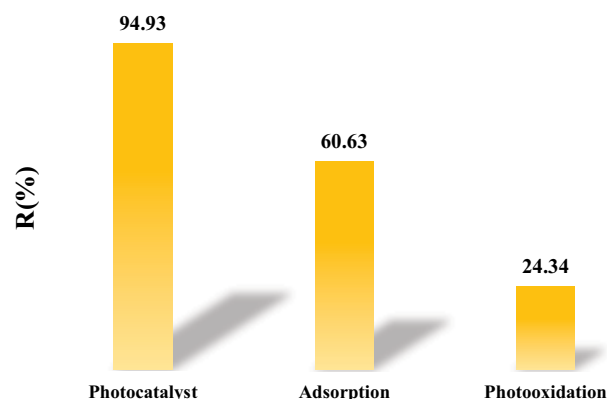
Fig. 11. Comparison of tetracycline removal in different processes.

4. Conclusion

In this study, we synthesized a new magnetic activated carbon nanocomposite by coating the magnetic activated carbon (MAC) obtained from AGH with copper sulfide (CuS) and investigated its effectiveness in removing tetracycline (TC) from aqueous media under simulated sunlight (Xenon light) and the effect of pH, nanocomposite dose, and initial contaminants concentration on the process. The results of this study showed that the new MAC/CuS nanocomposite is highly effective in degrading TC. The photocatalytic degradation process was found to have 94.93% efficiency under optimal conditions (pH = 9, catalyst dose = 1.5 g/L, contaminant concentration = 20 mg/L, exposure time = 60min, ambient temperature). The TC removal ratio initially increased with increasing the nanocomposite dose but started to decrease once the dose was raised above a certain level. This can be attributed to the interference of nanocomposite particles with light penetration into the solution. The use of Xenon light alone did not have a significant impact on TC removal efficiency (less than 30%). The kinetics of the degradation process was found to follow the pseudo-first-order kinetic model. Stability and reuse tests performed in six cycles showed a very low-efficiency reduction, meaning that the nanocomposite can be reused many times in the TC removal process. Considering the high efficiency of the synthesized nanocomposite in the photocatalytic degradation of tetracycline, its relatively simple synthesis process, and the fact that it can be easily separated from the medium with an N_{42} magnet, it can serve as an excellent catalyst for the degradation and removal of organic pharmaceutical contaminants.

Acknowledgments

References

[1] S. Li, M. Cai, Y. Liu, J. Zhang, C. Wang, S. Zang, Y. Li, P. Zhang, X. Li, In situ construction of a C_3N_5 nanosheet/Bi_2WO_6 nanodot S-scheme heterojunction with enhanced structural defects for the efficient photocatalytic removal of tetracycline and Cr(VI), Inorg. Chem. Front., 9 (2022) 2479–2497.

[2] R. Daghrir, P. Drogui, Tetracycline antibiotics in the environment: a review, Environ. Chem. Lett., 11 (2013) 209–227.

[3] Y. Gao, Y. Li, L. Zhang, H. Huang, J. Hu, S.M. Shah, X. Su, Adsorption and removal of tetracycline antibiotics from aqueous solution by graphene oxide, J. Colloid Interface Sci., 368 (2012) 540–546.

[4] A. Tiwari, A. Shukla, D. Tiwari, S.-M. Lee, Au-nanoparticle/nanopillars TiO_2 meso-porous thin films in the degradation of tetracycline using UV-A light, J. Ind. Eng. Chem., 69 (2019) 141–152.

[5] Y. Wu, Q. Yue, Y. Gao, Z. Ren, B. Gao, Performance of bimetallic nanoscale zero-valent iron particles for removal of oxytetracycline, J. Environ. Sci., 69 (2018) 173–182.

[6] G. Yang, Q. Gao, S. Yang, S. Yin, X. Cai, X. Yu, S. Zhang, Y. Fang, Strong adsorption of tetracycline hydrochloride on magnetic carbon-coated cobalt oxide nanoparticles, Chemosphere, 239 (2020) 124831, doi: 10.1016/j.chemosphere.2019.124831.

[7] T. Saitoh, K. Shibata, K. Fujimori, Y. Ohtani, Rapid removal of tetracycline antibiotics from water by coagulation–flotation of sodium dodecyl sulfate and poly(allylamine hydrochloride) in the presence of Al(III) ions, Sep. Purif. Technol., 187 (2017) 76–83.

[8] Y. Zhang, J. Zhou, X. Chen, L. Wang, W. Cai, Coupling of heterogeneous advanced oxidation processes and photocatalysis in efficient degradation of tetracycline hydrochloride by Fe-based MOFs: synergistic effect and degradation pathway, J. Chem. Eng., 369 (2019) 745–757.

[9] F. Deng, L. Zhao, X. Luo, S. Luo, D.D. Dionysiou, Highly efficient visible-light photocatalytic performance of Ag/$AgIn_5S_8$ for degradation of tetracycline hydrochloride and treatment of real pharmaceutical industry wastewater, J. Chem. Eng., 333 (2018) 423–433.

[10] L. Lan, X. Kong, H. Sun, C. Li, D. Liu, High removal efficiency of antibiotic resistance genes in swine wastewater via nanofiltration and reverse osmosis processes, J. Environ. Manage., 231 (2019) 439–445.

[11] W. Xiong, G. Zeng, Z. Yang, Y. Zhou, C. Zhang, M. Cheng, Y. Liu, L. Hu, J. Wan, C. Zhou, Adsorption of tetracycline antibiotics from aqueous solutions on nanocomposite multi-walled carbon nanotube functionalized MIL-53 (Fe) as new adsorbent, Sci. Total Environ., 627 (2018) 235–244.

[12] Z. Fang, J. Chen, X. Qiu, X. Qiu, W. Cheng, L. Zhu, Effective removal of antibiotic metronidazole from water by nanoscale zero-valent iron particles, Desal. Water Treat., 268 (2011) 60–67.

[13] V. Homem, L. Santos, Degradation and removal methods of antibiotics from aqueous matrices–a review, J. Environ. Manage., 92 (2011) 2304–2347.

[14] M.S. Abdel-Aziz, K.S. Abou-El-Sherbini, E.M.A. Hamzawy, M.H.A. Amr, S. El-Dafrawy, Green synthesis of silver nano-particles by *Macrococcus bovicus* and its immobilization onto montmorillonite clay for antimicrobial functionality, Appl. Biochem. Biotechnol., 176 (2015) 2225–2241.

[15] G. Sharma, D.D. Dionysiou, S. Sharma, A. Kumar, H. Ala'a, Mu. Naushad, F.J. Stadler, Highly efficient Sr/Ce/activated carbon bimetallic nanocomposite for photoinduced degradation of Rhodamine B, Catal. Today, 335 (2019) 437–451.

[16] Y.-Y. Yang, C.-G. Niu, X.-J. Wen, L. Zhang, C. Liang, H. Guo, D.-L. Guan, H.-Y. Liu, G.-M. Zeng, Fabrication of visible-light-driven silver iodide modified iodine-deficient bismuth oxyiodides Z-scheme heterojunctions with enhanced photocatalytic activity for *Escherichia coli* inactivation and tetracycline degradation, J. Colloid Sci., 533 (2019) 636–648.

[17] G. Sharma, A. Kumar, Mu. Naushad, A. Kumar, H. Ala'a, P. Dhiman, A.A. Ghfar, F.J. Stadler, M. Khan, Photoremediation of toxic dye from aqueous environment using monometallic and bimetallic quantum dots based nanocomposites, J. Cleaner Prod., 172 (2018) 2919–2930.

[18] G. Sharma, A. Kumar, S. Sharma, Mu. Naushad, P. Dhiman, D.-V.N. Vo, F.J. Stadler, $Fe_3O_4/ZnO/Si_3N_4$ nanocomposite based photocatalyst for the degradation of dyes from aqueous solution, Mater. Lett., 278 (2020) 128359, doi: 10.1016/j.matlet.2020.128359.

[19] Y. Li, M. Fu, R. Wang, S. Wu, X. Tan, Efficient removal TC by $Zn@SnO_2/PI$ via the synergy of adsorption and photocatalysis under visible light, J. Chem. Eng., 444 (2022) 136567, doi: 10.1016/j.cej.2022.136567.

[20] X. Zhang, N. Yuan, Y. Li, L. Han, Q. Wang, Fabrication of new MIL-53(Fe)@TiO_2 visible-light responsive adsorptive photocatalysts for efficient elimination of tetracycline, J. Chem. Eng., 428 (2022) 131077, doi: 10.1016/j.cej.2021.131077.

[21] X. Deng, D. Wang, H. Li, W. Jiang, T. Zhou, Y. Wen, B. Yu, G. Che, L. Wang, Boosting interfacial charge separation and photocatalytic activity of 2D/2D g-$C_3N_4/ZnIn_2S_4$ S-scheme heterojunction under visible light irradiation, J. Alloys Compd., 894 (2022) 162209, doi: 10.1016/j.jallcom.2021.162209.

[22] A. Reheman, K. Kadeer, K. Okitsu, M. Halidan, Y. Tursun, T. Dilinuer, A. Abulikemu, Facile photo-ultrasonic assisted reduction for preparation of rGO/Ag_2CO_3 nanocomposites with enhanced photocatalytic oxidation activity for tetracycline, Ultrason. Sonochem., 51 (2019) 166–177.

[23] A. Assadi, M.H. Dehghani, N. Rastkari, S. Nasseri, A.H. Mahvi, Photocatalytic reduction of hexavalent chromium in aqueous solutions with zinc oxide nanoparticles and hydrogen peroxide, Environ. Prot. Eng., 38 (2012) 5–16.

[24] X. Bai, Y.J. Wang, Y. Li, X.J. Wang, Adsorption–photocatalytical remediation for series of tetracycline contaminants with BiOCl–CdS composite under simulated sunlight, J. Taiwan Inst. Chem. Eng., 104 (2019) 94–105.

[25] N. Farhadian, R. Akbarzadeh, M. Pirsaheb, T.-C. Jen, Y. Fakhri, A. Asadi, Chitosan modified N, S-doped TiO_2 and N, S-doped ZnO for visible light photocatalytic degradation of tetracycline, Int. J. Biol. Macromol., 132 (2019) 360–373.

[26] Q. Wu, Z. Zhang, The fabrication of magnetic recyclable nitrogen modified titanium dioxide/strontium ferrite/diatomite heterojunction nanocomposite for enhanced visible-light-driven photodegradation of tetracycline, Int. J. Hydrogen Energy, 44 (2019) 8261–8272.

[27] A. Kumar, S.K. Sharma, G. Sharma, C. Guo, D.-V.N. Vo, J. Iqbal, Mu. Naushad, F.J. Stadler, Silicate glass matrix@$Cu_2O/Cu_2V_2O_7$ p-n heterojunction for enhanced visible light photodegradation of sulfamethoxazole: high charge separation and interfacial transfer, J. Hazard. Mater., 402 (2021) 123790, doi: 10.1016/j.jhazmat.2020.123790.

[28] P. Dhiman, Mu. Naushad, K.M. Batoo, A. Kumar, G. Sharma, A.A. Ghfar, G. Kumar, M. Singh, Nano $Fe_xZn_{1-x}O$ as a tuneable and efficient photocatalyst for solar powered degradation of bisphenol A from aqueous environment, J. Cleaner Prod., 165 (2017) 1542–1556.

[29] A. Ahmad, M. Ali, A.G. Al-Sehemi, A.A. Al-Ghamdi, J.-W. Park, H. Algarni, H. Anwer, Carbon-integrated semiconductor photocatalysts for removal of volatile organic compounds in indoor environments, J. Chem. Eng., 452 (2023) 139436, doi: 10.1016/j.cej.2022.139436.

[30] C. Zhao, W. Yin, J. Xu, Y. Zhang, D. Shang, Z. Guo, Q. Wang, J. Wang, Q. Kong, Removal of tetracycline from water using activated carbon derived from the mixture of *Phragmites australis* and waterworks sludge, ACS Omega, 5 (2020) 16045–16052.

[31] L. Ai, J. Jiang, Fast removal of organic dyes from aqueous solutions by AC/ferrospinel composite, Desal. Water Treat., 262 (2010) 134–140.

[32] D. Mohan, A. Sarswat, V.K. Singh, M. Alexandre-Franco, C.U. Pittman Jr., Development of magnetic activated carbon from almond shells for trinitrophenol removal from water, J. Chem. Eng., 172 (2011) 1111–1125.

[33] G. Sharma, A. Kumar, S. Sharma, H. Ala'a, Mu. Naushad, A.A. Ghfar, T. Ahamad, F.J. Stadler, Fabrication and characterization of novel Fe^0@guar gum-crosslinked-soya lecithin nanocomposite hydrogel for photocatalytic degradation of methyl violet dye, Sep. Purif. Technol., 211 (2019) 895–908.

[34] B. Kakavandi, A. Jonidi Jafari, R. Rezaei Kalantary, S. Nasseri, A. Ameri, A. Esrafily, Synthesis and properties of Fe_3O_4-activated carbon magnetic nanoparticles for removal of aniline from aqueous solution: equilibrium, kinetic and thermodynamic studies, Iran. J. Environ. Health Sci. Eng., 10 (2013) 19, doi: 10.1186/1735-2746-10-19.

[35] X.S. Wang, Y. Zhou, Y. Jiang, C. Sun, The removal of basic dyes from aqueous solutions using agricultural by-products, J. Hazard. Mater., 157 (2008) 374–385.

[36] S. Sutar, S. Otari, J. Jadhav, Biochar based photocatalyst for degradation of organic aqueous waste: a review, Chemosphere, 287 (2022) 132200, doi: 10.1016/j.chemosphere.2021.132200.

[37] M.R. Assalin, V.L. Ferracini, S.C.N. Queiroz, C.M. Jonsson, Z. Clemente, S.R. Silva, Photocatalytic degradation of an organophosphorus pesticide from agricultural waste by immobilized TiO_2 under solar radiation, Rev. Ambient. Água, 11 (2016) 778–787.

[38] N. Nasseh, R. Khosravi, N.s. Mazari Moghaddam, S. Rezania, Effect of UV_C and UV_A photocatalytic processes on tetracycline removal using CuS-coated magnetic activated carbon nanocomposite: a comparative study, Int. J. Environ. Res. Public Health, 18 (2021) 11163, doi: 10.3390/ijerph182111163.

[39] Q. Liu, L.-B. Zhong, Q.-B. Zhao, C. Frear, Y.-M. Zheng, Synthesis of Fe_3O_4/polyacrylonitrile composite electrospun nanofiber mat for effective adsorption of tetracycline, ACS Appl. Mater. Interfaces, 7 (2015) 14573–14583.

[40] A.-A. Salarian, Z. Hami, N. Mirzaei, S.M. Mohseni, A. Asadi, H. Bahrami, M. Vosoughi, A. Alinejad, M.-R. Zare, N-doped TiO_2 nanosheets for photocatalytic degradation and mineralization of diazinon under simulated solar irradiation: optimization and modeling using a response surface methodology, J. Mol. Liq., 220 (2016) 183–191.

[41] B. Kakavandi, A. Takdastan, N. Jaafarzadeh, M. Azizi, A. Mirzaei, A. Azari, Application of Fe_3O_4@C catalyzing heterogeneous UV-Fenton system for tetracycline removal with a focus on optimization by a response surface method, J. Photochem. Photobiol., A, 314 (2016) 178–188.

[42] W.E. Federation, A. Association, Standard Methods for the Examination of Water and Wastewater, American Public Health Association (APHA), Washington, D.C., USA, 2005.

[43] W. Jiang, Z. Li, C. Liu, D. Wang, G. Yan, B. Liu, G. Che, Enhanced visible-light-induced photocatalytic degradation of tetracycline using BiOI/MIL-125(Ti) composite photocatalyst, J. Alloys Compd., 854 (2021) 157166, doi: 10.1016/j.jallcom.2020.157166.

[44] V.R. Chelli, A.K. Golder, Ag-doping on ZnO support mediated by bio-analytes rich in ascorbic acid for photocatalytic degradation of dipyrone drug, Chemosphere, 208 (2018) 149–158.

[45] C. Gómez-Pacheco, M. Sánchez-Polo, J. Rivera-Utrilla, J. López-Peñalver, Tetracycline degradation in aqueous phase by ultraviolet radiation, J. Chem. Eng., 187 (2012) 89–95.

[46] J.J. López-Peñalver, M. Sánchez-Polo, C.V. Gómez-Pacheco, J. Rivera-Utrilla, Photodegradation of tetracyclines in aqueous solution by using UV and UV/H_2O_2 oxidation processes, J. Chem. Technol. Biotechnol., 85 (2010) 1325–1333.

[47] H.U. Rasheed, X. Lv, W. Wei, D.K. Sam, N. Ullah, J. Xie, W. Zhu, Highly efficient photocatalytic degradation of the tetracycline hydrochloride on the α-Fe_2O_3@CN composite under the visible light, J. Environ. Chem. Eng., 7 (2019) 103322, doi: 10.1016/j.jece.2019.103322.

[48] J. Pablos, C. Abrusci, I. Marín, J. López-Marín, F. Catalina, E. Espí, T. Corrales, Photodegradation of polyethylenes: comparative effect of Fe and Ca-stearates as pro-oxidant additives, Polym. Degrad. Stab., 95 (2010) 2057–2064.

[49] Z. Xue, T. Wang, B. Chen, T. Malkoske, S. Yu, Y. Tang, Degradation of tetracycline with $BiFeO_3$ prepared by a simple hydrothermal method, J. Mater., 8 (2015) 6360–6378.

[50] Y. Ma, N. Gao, C. Li, Degradation and pathway of tetracycline hydrochloride in aqueous solution by potassium ferrate, Environ. Eng. Sci., 29 (2012) 357–362.

[51] G. Safari, M. Hoseini, M. Seyedsalehi, H. Kamani, J. Jaafari, A. Mahvi, Photocatalytic degradation of tetracycline using nanosized titanium dioxide in aqueous solution, Int. J. Environ. Sci. Technol., 12 (2015) 603–616.

[52] P. Wang, P.-S. Yap, T.-T. Lim, C–N–S tri-doped TiO_2 for photocatalytic degradation of tetracycline under visible-light irradiation, Appl. Catal., 399 (2011) 252–261.

[53] Y. Wang, H. Zhang, L. Chen, Ultrasound enhanced catalytic ozonation of tetracycline in a rectangular air-lift reactor, Catal. Today, 175 (2011) 283–292.

[54] Y. Wang, H. Zhang, J. Zhang, C. Lu, Q. Huang, J. Wu, F. Liu, Degradation of tetracycline in aqueous media by ozonation in an internal loop-lift reactor, J. Hazard. Mater., 192 (2011) 35–43.

[55] G. Sharma, A. Kumar, Mu. Naushad, B. Thakur, D.-V.N. Vo, B. Gao, A.A. Al-Kahtani, F.J. Stadler, Adsorptional-photocatalytic removal of fast sulphon black dye by using chitin-cl-poly(itaconic acid-*co*-acrylamide)/zirconium tungstate nanocomposite hydrogel, J. Hazard. Mater., 416 (2021) 125714, doi: 10.1016/j.jhazmat.2021.125714.

[56] C.-C. Liu, Y.-H. Hsieh, P.-F. Lai, C.-H. Li, C.-L. Kao, Photodegradation treatment of azo dye wastewater by UV/TiO_2 process, Dyes Pigm., 68 (2006) 191–195.

[57] A. Eslami, M.M. Amini, A.R. Yazdanbakhsh, A. Mohseni-Bandpei, A.A. Safari, A. Asadi, N, S co-doped TiO_2 nanoparticles and nanosheets in simulated solar light for photocatalytic degradation of non-steroidal anti-inflammatory drugs in water: a comparative study, J. Chem. Technol. Biotechnol., 91 (2016) 2693–2704.

[58] J. Rashid, M. Barakat, Y. Ruzmanova, A. Chianese, Fe_3O_4/SiO_2/TiO_2 nanoparticles for photocatalytic degradation of 2-chlorophenol in simulated wastewater, Environ. Sci. Pollut. Res., 22 (2015) 3149–3157.

[59] E.S. Elmolla, M. Chaudhuri, Photocatalytic degradation of amoxicillin, ampicillin and cloxacillin antibiotics in aqueous solution using UV/TiO_2 and $UV/H_2O_2/TiO_2$ photocatalysis, Desal. Water Treat., 252 (2010) 46–52.

[60] S. Ahmed, M. Rasul, R. Brown, M. Hashib, Influence of parameters on the heterogeneous photocatalytic degradation of pesticides and phenolic contaminants in wastewater: a short review, J. Environ. Manage., 92 (2011) 311–330.

[61] S.S. Rezaei, B. Kakavandi, M. Noorisepehr, A.A. Isari, S. Zabih, P. Bashardoust, Photocatalytic oxidation of tetracycline by magnetic carbon-supported TiO_2 nanoparticles catalyzed peroxydisulfate: performance, synergy and reaction mechanism studies, Sep. Purif. Technol., 258 (2021) 117936, doi: 10.1016/j.seppur.2020.117936.

[62] R. Nosrati, A. Olad, R. Maramifar, Degradation of ampicillin antibiotic in aqueous solution by ZnO/polyaniline nanocomposite as photocatalyst under sunlight irradiation, Environ. Sci. Pollut. Res. Int., 19 (2012) 2291–2299.

[63] G.H. Safari, M. Hoseini, H. Kamali, R. Moradirad, A.H. Mahvi, Photocatalytic degradation of tetracycline antibiotic from aqueous solutions using UV/TiO_2 and $UV/H_2O_2/TiO_2$, J. Health: Ardabil Univ. Med. Sci., 5 (2014) 203–2013.

[64] D. Dimitrakopoulou, I. Rethemiotaki, Z. Frontistis, N.P. Xekoukoulotakis, D. Venieri, D. Mantzavinos, Degradation, mineralization and antibiotic inactivation of amoxicillin by UV-A/TiO_2 photocatalysis, J. Environ. Manage., 98 (2012) 168–174.

[65] M. Zhang, W. Song, Q. Chen, B. Miao, W. He, One-pot synthesis of magnetic $Ni@Mg(OH)_2$ core–shell nanocomposites as a recyclable removal agent for heavy metals, ACS Appl. Mater. Interfaces, 7 (2015) 1533–1540.

[66] L.S. Lam, Photocatalytic Degradation of Sunset Yellow Dye over Zinc Oxide Nanoparticles under Fluorescent Light Irradiation, A Project Report Submitted in Partial Fulfilment of the Requirements for the Award of Bachelor of Engineering (Hons) Petrochemical Engineering, University Tunku Abdul Rahman, 2016.

[67] Z. Lu, X. Zhao, Z. Zhu, Y. Yan, W. Shi, H. Dong, Z. Ma, N. Gao, Y. Wang, H. Huang, Enhanced recyclability, stability, and selectivity of $CdS/C@Fe_3O_4$ nanoreactors for orientation photodegradation of ciprofloxacin, Eur. J. Chem., 21 (2015) 18528–18533.

[68] N. Nasseh, A.H. Panahi, M. Esmati, N. Daglioglu, A. Asadi, H. Rajati, F. Khodadoost, Enhanced photocatalytic degradation of tetracycline from aqueous solution by a novel magnetically separable $FeNi_3/SiO_2/ZnO$ nanocomposite under simulated sunlight: efficiency, stability, and kinetic studies, J. Mol. Liq., 301 (2020) 112434, doi: 10.1016/j.molliq.2019.112434.

[69] X.-X. Zhang, X.-J. Wang, Y.-Y. Niu, Photocatalytic degradation of tetracycline by supramolecular materials constructed with organic cations and silver iodide, J. Catal., 12 (2022) 1581, doi: 10.3390/catal12121581.